

## Article

# Dynamic Surface-Based Adaptive Active Disturbance Rejection Control of Electrohydrostatic Actuators

Xudong Han <sup>1</sup>, Yongling Fu <sup>1</sup>, Yan Wang <sup>2,\*</sup>, Mingkang Wang <sup>1</sup> and Deming Zhu <sup>3</sup>

<sup>1</sup> School of Mechanical Engineering and Automation, Beihang University, Beijing 100191, China; xdhan@buaa.edu.cn (X.H.)

<sup>2</sup> School of Transportation Science and Engineering, Beihang University, Beijing 100191, China

<sup>3</sup> Engineering Training Center, Beihang University, Beijing 102206, China

\* Correspondence: wybuaa@buaa.edu.cn

**Abstract:** The control accuracy and stability of the electrohydrostatic actuator (EHA) are directly impacted by parameter uncertainty, disturbance uncertainty, and non-matching disturbance, which negatively impacts aircraft rudder maneuvering performance and even results in rudder chatter. A dynamic surface-based adaptive active disturbance rejection control (DSAADRC) is proposed as a solution for these issues. It does this by developing a novel parametric adaptive law driven by the combination of tracking error, parameter estimation error, and state estimation error to estimate the unknown parameters, using three low-order ESOs to estimate and compensate the uncertain disturbances online, and employing a dynamic surface method to obtain the differential values of virtual control signals in the backstepping method to deal with non-matching disturbances. In this research, a Lyapunov stability analysis demonstrates that the method can achieve the position tracking accuracy of the EHA under time-varying external disturbances after first establishing an EHA dynamics model with nonlinearity and uncertainty, followed by the design of an adaptive active disturbance rejection control method based on dynamic surfaces for the uncertainties and perturbations. In contrast to control strategies like Robust Control (RC) and Adaptive Robust Control (ARC), simulation and experiment comparison shows that the method has stronger anti-disturbance under time-varying external disturbances.



**Citation:** Han, X.; Fu, Y.; Wang, Y.; Wang, M.; Zhu, D. Dynamic Surface-Based Adaptive Active Disturbance Rejection Control of Electrohydrostatic Actuators.

*Aerospace* **2023**, *10*, 747. <https://doi.org/10.3390/aerospace10090747>

Academic Editor: Konstantinos Kontis

Received: 8 July 2023

Revised: 13 August 2023

Accepted: 18 August 2023

Published: 23 August 2023



**Copyright:** © 2023 by the authors. Licensee MDPI, Basel, Switzerland. This article is an open access article distributed under the terms and conditions of the Creative Commons Attribution (CC BY) license (<https://creativecommons.org/licenses/by/4.0/>).

**Keywords:** electrohydrostatic actuator (EHA); adaptive robust control (ARC); extended state observer (ESO); dynamic surface control

## 1. Introduction

With the development of power-by-wire (PBW) technology in the aerospace field, the flight actuation system is gradually replacing conventional power-by-pipe actuation with electrical actuation for primary and key secondary flight controls [1,2]. A novel actuator for more electric aircraft, the Electro-Hydrostatic Actuator (EHA) consists of an electronic control unit, a servo motor, a hydraulic pump, a cylinder, and hydraulic auxiliary components. It has been used in several aircraft models to drive critical rudder surfaces, such as the F-35 fighter, A350, and A380 commercial aircraft [2]. Generally, according to the working principle, EHA can be divided into three types: EHA with fixed-displacement pump and variable-speed motor (EHA-FPVM) [3], EHA with variable-displacement pump and fixed-speed motor [4], and EHA with variable-displacement pump and variable-speed motor (EHA-VPVM) [5,6].

EHAs have the benefits of high efficiency, high integration, small size, and light weight [1,7], but they also have parameter uncertainties, disturbance uncertainties, and nonmatching disturbances. For example, internal friction and leakage, as well as external load uncertainties, are nonlinear disturbances, and the channels through which they enter the system are different from the channels through which the control input signals enter [8,9].

Parameter uncertainties such as internal and external leakage coefficients and viscous friction coefficients pose certain difficulties for the design of model-based EHA controllers. The EHA parameters, which frequently deviate from the nominal values during actual operation due to temperature, operating conditions, and other perturbations, strongly influence the control input designed based on model information. If the control law designed according to the nominal parameters is implemented without considering the parameter variations, it will increase the tracking error. Wang et al. suggested a combination of variable structure filter and sliding mode control to deal with bounded parameter uncertainty and noise in EHAs [10], and Lee et al. combined the advantages of adaptive PID and sliding mode control to design an adaptive anti-saturation sliding mode controller for suppressing parameter vagueness in EHAs [11]. Ahn et al. combined an adaptive law and an improved backstepping method to compensate for parameter uncertainty in EHA systems [12], but the approach has trouble dealing with outside disturbances.

The EHA also has a significant amount of disturbance uncertainty, which includes external load uncertainty as well as nonlinear disturbances within the system, like leakage and friction characteristics of hydraulic pumps and cylinders. Because their perturbation forms and the nonlinear functions that can accurately describe their characteristics are unknown, these characteristics are difficult to model accurately, which results in the controller's performance under actual operation degrading or even becoming unstable, which affects the accuracy of the EHA position tracking [13]. Sliding mode control, as a robust control technique with strict theoretical support, has many applications in EHA control because it can successfully handle uncertain nonlinearities and achieve asymptotic stability [8,10,14]. However, the chattering problem in sliding mode control has been a concern. Yang et al. designed a sliding mode observer and a new convergence law to eliminate chattering [15], but the approach is too complex to be used. Yao et al. proposed an adaptive robust control (ARC) strategy integrating backstepping and the adaptive method [16], and this procedure proved its effectiveness in the control of both valve-controlled cylinders and hydraulic motors [17,18]. High feedback gains are produced as a result of the technique's excessive reliance on the robust term's ability to counteract external disturbances, which can excite the system's unmodeled dynamics and lead to instability [19].

Compared to matching disturbances, non-matching disturbances enter the system on a different channel than the control input, which makes it impossible to compensate for them with a conventional feedforward controller. In order to suppress non-matching disturbances, a number of improved sliding mode controllers have been proposed [20,21]. However, these techniques require that the non-matching disturbances satisfy the assumption that the amplitude tends to zero at infinity, which is challenging to accomplish in the majority of real-world systems. Yang et al. proposed a robust control system based on a nonlinear disturbance observer that can suppress the effects of nonmatching disturbances and parameter variations from the system output channel [22]. To address the disturbance suppression issue for non-integral-chain systems with mismatched uncertainties, Li et al. proposed generalized ESO-based control methods [23]. However, the estimation peaking phenomenon of disturbances generated in this type of method can cause control peaking phenomenon under high observation gain conditions, resulting in unstable control quantities [24]. In order to deal with non-matching uncertainties like dead zones in EHAs and achieve global stability, Yang et al. adopted the adaptive backstepping method [25]. But, since EHA is a high-order system, the increase in variables in the virtual control signals leads to the final control input comprising multi-order partial differentiation, which is difficult to apply practically. Many corresponding solutions have been proposed for the "differential explosion" problem, such as dynamic surface control (DSC) [26,27], command-filtered backstepping control (CFBC) [28–30], etc. On the other hand, supersonic vehicle attitude adjustment is where such control methods are most frequently used [31–33]. For high-order EHA systems, the use of dynamic surface control to solve the "differential explosion" problem, together with active compensation control to suppress the uncertainty, has rarely been mentioned.

In overall review, the parameter uncertainty, disturbance uncertainty, and non-matching disturbance of EHAs pose great difficulties for their high-precision motion control. Many studies have been performed on high-precision EHA control strategies, with the majority of them concentrating on the suppression of a particular kind of disturbance. The above three types of problems can all be solved simultaneously, but there have not been many studies that successfully apply the solutions to real-world situations. Therefore, it is necessary to design control strategies for EHA that simultaneously solve parameter uncertainty, disturbance uncertainty, and non-matching disturbance to ensure high precision control.

This paper suggests a Dynamic Surface based Adaptive Active Disturbance Rejection control (DSAADRC) method for the issues with EHA in light of the aforementioned considerations. A novel parametric adaptive law driven by a combination of tracking error, parameter estimation error, and state estimation error is also constructed and made to combine with a multi-stage extended state observer. The method is able to adapt to the unknown parameters while actively compensating for the matching and nonmatching disturbances in the system. The differential value of the virtual control signals is also obtained because the EHA is a fourth-order system by introducing a dynamic surface for the backstepping “differential explosion” problem. This prevents the control law’s multi-order partial differentiation and successfully integrates the extended state observer, the ARC method, and the dynamic surface. In the presence of time-varying disturbances, the ultimately uniform boundedness of the system’s position tracking is still guaranteed. The contributions of this paper lie in the following aspects:

- (1) A novel method is proposed to deal with the problem of parameter uncertainty and uncertain perturbation in high-order systems. The novel adaptive law driven by tracking error, parameter estimation error, and state estimation error reduces the burden of ESOs, and the dynamic surface method makes it effectively applied to high-order systems. Compared with the current studies, the effective fusion of the three methods is realized, and the stability analysis proves that all signals in the system are bounded.
- (2) The proposed control strategy is applied to the position servo control of EHA, and sufficient simulation and experimental results verify the effectiveness of the control strategy.

This paper is organized as follows: first, a description of the EHA’s nonlinear modeling; second, a description of the DSAADRC method’s design process; and third, a demonstration of its Lyapunov stability. The next step involves simulation and experimental validation. The position tracking performance of three controllers, DSAADRC, Adaptive Robust Control (ARC), and Robust Control (RC), is compared based on the established non-linear model of EHA to confirm the efficacy of the control strategy suggested in this paper with conclusions.

## 2. EHA System Description

Figure 1 illustrates the EHA’s operational theory. In response to the host computer’s command, the drive controller activates the servo motor, which in turn activates the bi-directional pump. The expansion and contraction of the acting cylinder are made possible by the injection of oil into the cylinder through the hydraulic circuit. In this manner, the specified position for the controlled rudder surface is pushed, so that the entire EHA system realizes the function of manipulating the rudder surface position to follow the control command. Among them, the regulating valve is used to bypass the two chambers of the cylinder in the case of rudder surface jamming, so that the actuator can be in a follow-up mode to avoid the failure of the aircraft’s flight control system.

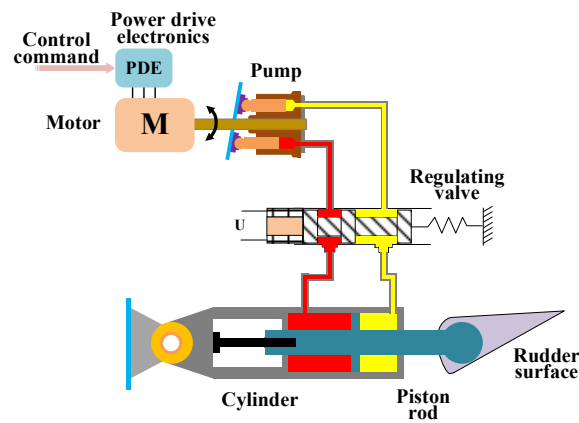


**Figure 1.** Schematic diagram of an EHA.

### 2.1. Model of Brushless DC Motor (BLDCM)

The servo motor used by EHA is a brushless DC motor. Because the motor's electrical response is much faster than the mechanical response, its characteristics are treated as a proportional link, that is  $U = k_e\omega + Ri$ . Consequently, the brushless DC motor is treated as a first-order link with the bus voltage  $U$  as input and the spindle speed  $\omega$  as output. The dynamic equation is given by the following:

$$\begin{cases} U = k_e\omega + Ri \\ T_e = k_t i \\ J_m \dot{\omega} = T_e - T_L - B_m\omega - T_f \end{cases} \quad (1)$$

where  $k_e$  and  $k_t$  are the back EMF and torque coefficients, respectively;  $R$  is the equivalent resistance;  $i$  is the bus current;  $T_e$  is the electromagnetic torque;  $J_m$  is the rotational inertia;  $T_L$  is the equivalent external load;  $B_m$  is the viscous friction coefficient; and  $T_f$  is the static friction.

### 2.2. Pump-Controlled Hydraulic Cylinder Model

The hydraulic pump's inlet and outlet flow rates are determined by the hydraulic pump's working principle, as follows:

$$\begin{cases} Q_i = \omega D_p - L_i(p_i - p_o) - L_o(p_i - p_a) - \frac{V_{in}}{\beta_e} \dot{p}_i \\ Q_o = \omega D_p - L_i(p_i - p_o) + L_o(p_o - p_a) + \frac{V_{out}}{\beta_e} \dot{p}_o \end{cases} \quad (2)$$

where  $Q_i$  and  $Q_o$  are hydraulic pump's inlet and outlet flow rates, respectively;  $D_p$  is the discharge volume;  $L_i$  is the internal leakage coefficient;  $L_o$  is the external leakage coefficient;  $p_i$ ,  $p_o$ , and  $p_a$  are the inlet pressure, outlet pressure, and tank pressure;  $V_{in}$  and  $V_{out}$  are the equivalent volume of the inlet and outlet chambers; and  $\beta_e$  is the elastic modulus of the fluid.

The hydraulic cylinder's dynamic equation is as follows:

$$\begin{cases} Q_l = A\dot{x} + \frac{V_{in}}{\beta_e} \frac{dp_l}{dt} + L_c(p_l - p_r) \\ Q_r = A\dot{x} - \frac{V_{out}}{\beta_e} \frac{dp_r}{dt} - L_c(p_l - p_r) \end{cases} \quad (3)$$

where  $Q$  and  $p$  represent the flow rate and pressure of the corresponding chamber, the subscripts  $l$  and  $r$  denote the left and right chambers of the cylinder, respectively;  $A$  is the effective area of the piston;  $x$  is the piston displacement; and  $L_c$  is the cylinder's internal leakage coefficient.

Neglecting the pressure drop loss in the valve block, by the flow continuity theorem, it is known that  $Q_l = Q_i$  and  $Q_r = Q_o$ . Combining Equations (2) and (3), the model of the pump and cylinder can be expressed as follows:

$$\begin{cases} D_p \omega = A \dot{x} + \frac{V_0}{\beta_e} \Delta \dot{p} + L_a \Delta p + Q_a \\ A \Delta p = M \ddot{x} + B_c \dot{x} + K_s x + F_f + F_L \end{cases} \quad (4)$$

where  $V_0$  is the effective volume of the chamber;  $L_a$  is the total leakage coefficient of the pump and cylinder, which is proportional to the difference in pressure  $\Delta p$ ;  $Q_a$  is the unpredictable flow loss;  $M$  is the total equivalent mass of the cylinder and load;  $B_c$  is the viscous friction coefficient of the cylinder;  $K_s$  is the elastic load coefficient; and  $F_f$  and  $F_L$  are the static friction and external load, respectively.

By combining Equations (1) and (4) and choosing the system state variable as  $X = [x_1 \ x_2 \ x_3 \ x_4]^T = [x \ \dot{x} \ \Delta p \ \omega]^T$ , the state space equation of the EHA can be established as follows:

$$\begin{cases} \dot{x}_1 = x_2 \\ \dot{x}_2 = \frac{A}{M} x_3 - \frac{B_c}{M} x_2 - \frac{F_f + F_L}{M} \\ \dot{x}_3 = \frac{\beta_e}{V_0} (D_p x_4 - A x_2 - L_c x_3 - Q_{un}) \\ \dot{x}_4 = \frac{1}{J_a} (k_t \frac{U - k_e x_4}{R} - B_m x_4 - D_p x_3 - T_f) \end{cases} \quad (5)$$

where  $J_a$  is the total rotational inertia of the pump and motor; and  $Q_{un}$  is the unpredictable flow loss.

### 3. Controller Design

#### 3.1. Problem Description

From Equation (5), it is known that the EHA is a fourth-order system with bus voltage  $U$  as input and piston rod displacement  $x_1$  as output. There are unknown external disturbances in the system, such as the external load force of the hydraulic cylinder  $F_L$ , the immeasurable flow loss  $Q_{un}$  including the leakage flow inside and outside the pump, and the static friction torque of the motor shaft  $T_f$ , which are all unpredictable and difficult to obtain their dynamic characteristics, and parameter uncertainty, reflected in the fact that the true values of  $B_c$ ,  $L_c$ ,  $B_m$  are not known. They are time-varying due to factors such as temperature and hydraulic system pressure. All these factors pose challenges to model-based control law design.

Redefine the vector of unknown parameters as follows:

$$\theta = [\theta_1, \theta_2, \theta_3]^T = \left[ \frac{B_c}{M}, \frac{\beta_e L_c}{V_0}, \frac{B_m}{J_a} \right]^T.$$

Then, Equation (5) can be rewritten as follows:

$$\begin{cases} \dot{x}_1 = x_2 \\ \dot{x}_2 = \frac{A}{M} x_3 - \theta_1 x_2 - F(t) \\ \dot{x}_3 = \frac{\beta_e D_p}{V_0} x_4 - \frac{\beta_e A}{V_0} x_2 - \theta_2 x_3 - Q(t) \\ \dot{x}_4 = \frac{k_t}{R J_a} (U - k_e x_4) - \frac{D_p}{J_a} x_3 - \theta_3 x_4 - T(t) \end{cases} \quad (6)$$

In Equation (6),  $F(t) = (F_f + F_L)/M$ ,  $T(t) = T_f/J_a$ , and  $Q(t) = Q_{un}\beta_e/V_0$ . It is crucial to remember that even though the parameter's true value is unknown, its upper and lower bounds are simple to determine:

$$\theta \in \Omega_\theta = \{ \theta : \theta_{\min} \leq \theta \leq \theta_{\max} \}$$

where  $\begin{cases} \theta_{\min}^T = [\theta_{1\min} \ \theta_{2\min} \ \theta_{3\min}]^T \\ \theta_{\max}^T = [\theta_{1\max} \ \theta_{2\max} \ \theta_{3\max}]^T \end{cases}$  denotes the minimum and maximum values of the known parameters, respectively.

### 3.2. Nonlinear Projection Design

Design Proj(\*) as a nonlinear projection, denoted as follows:

$$\text{Proj}_{\hat{\theta}_i}(\bullet_i) = \begin{cases} 0, & \text{if } \hat{\theta}_i > \theta_{i\max} \text{ and } \dot{\hat{\theta}}_i > 0 \\ 0, & \text{if } \hat{\theta}_i < \theta_{i\min} \text{ and } \dot{\hat{\theta}}_i < 0 \\ \bullet_i, & \text{else} \end{cases} \quad (7)$$

In Equation (7),  $i = 1, 2, 3$ . The adaptive law is designed as follows:

$$\dot{\hat{\theta}} = \text{Proj}(-\Gamma\omega), (\theta_{\min} \leq \theta(0) \leq \theta_{\max}) \quad (8)$$

In Equation (8),  $\Gamma$  and  $\omega$  are the diagonal gain matrix and the adaptive function to be designed, respectively. At this point, the following properties can be obtained:

$$\begin{cases} \theta \in \Omega_{\theta} = \{\theta : \theta_{\min} \leq \theta \leq \theta_{\max}\} \\ \hat{\theta}^T [\Gamma^{-1} \text{Proj}_{\hat{\theta}}(\Gamma\omega) - \omega] \leq 0 \end{cases} \quad (9)$$

### 3.3. Extended State Observer (ESO) Design

It is easy to find that the system states  $x_1, x_3$  and  $x_4$  are all measurable quantities in Equation (6). In order to estimate external disturbances, three extended state observers can be designed. One could infer the following:

$$\begin{cases} \dot{F}(t) = h_1(t) \\ \dot{Q}(t) = h_2(t) \ , \ h_i \leq |h_i|_{\max} \ (i = 1, 2, 3) \\ \dot{T}(t) = h_3(t) \end{cases} \quad (10)$$

Considering the perturbations  $F(t), Q(t)$ , and  $T(t)$  in the three subsystems, the three extended state observers are designed for their different subsystem orders:

$$\begin{cases} \dot{\hat{x}}_1 = \hat{x}_2 - 3\tau_1(\hat{x}_1 - x_1) \\ \dot{\hat{x}}_2 = \frac{A}{M}x_3 - \hat{\theta}_1x_2 - \hat{F}(t) - 3\tau_1^2(\hat{x}_1 - x_1) \\ \dot{\hat{F}}(t) = -\tau_1^3(\hat{x}_1 - x_1) \end{cases} \quad (11)$$

$$\begin{cases} \dot{\hat{x}}_3 = \frac{\beta_e}{V_0}(D_p x_4 - Ax_2) - \hat{\theta}_2x_3 - \hat{Q}(t) - 2\tau_2(\hat{x}_3 - x_3) \\ \dot{\hat{Q}}(t) = -\tau_2^2(\hat{x}_3 - x_3) \end{cases} \quad (12)$$

$$\begin{cases} \dot{\hat{x}}_4 = \frac{k_t}{R J_a}(U - k_e x_4) - \frac{D_p}{J_a}x_3 - \hat{\theta}_3x_4 - \hat{T}(t) - 2\tau_3(\hat{x}_4 - x_4) \\ \dot{\hat{T}}(t) = -\tau_3^2(\hat{x}_4 - x_4) \end{cases} \quad (13)$$

where  $\tau_i (i = 1, 2, 3)$  is the observer's adjustable parameter, which can be determined by the necessarily required bandwidth. The definition of the observation error is  $\tilde{\bullet} = \hat{\bullet} - \bullet$ . By differing the first two, third, and fourth equations of Equation (6) by Equations (11)–(13), the expression of the observed error is as follows:

$$\begin{cases} \dot{\eta}_1 = \tau_1 A_1 \eta_1 - B_1 \frac{\tilde{\theta}_1}{\tau_1} x_2 - B_2 \frac{h_1(t)}{\tau_1^2} \\ \dot{\eta}_2 = \tau_2 A_2 \eta_2 - C_1 \tilde{\theta}_2 x_3 - C_2 \frac{h_2(t)}{\tau_2} \\ \dot{\eta}_3 = \tau_3 A_3 \eta_3 - D_1 \tilde{\theta}_3 x_4 - D_2 \frac{h_3(t)}{\tau_3} \end{cases} \quad (14)$$

where  $\eta_1 = [\tilde{x}_1, \tilde{x}_2/\tau_1, \tilde{F}(t)/\tau_1^2]^T$ ,  $\eta_2 = [\tilde{x}_3, \tilde{Q}(t)/\tau_2]^T$ ,  $\eta_3 = [\tilde{x}_4, \tilde{T}(t)/\tau_3]^T$ ,  $B_1 = [0, 1, 0]^T$ ,  $B_2 = [0, 0, 1]^T$ ,  $C_1 = [1, 0]^T$ ,  $C_2 = [0, 1]^T$ ,  $D_1 = [1, 0]^T$ ,  $D_2 = [0, 1]^T$ , and  $A_1 = \begin{bmatrix} -3 & 1 & 0 \\ -3 & 0 & -1 \\ -1 & 0 & 0 \end{bmatrix}$ ,  $A_2 = \begin{bmatrix} -2 & -1 \\ -1 & 0 \end{bmatrix}$ ,  $A_3 = \begin{bmatrix} -2 & -1 \\ -1 & 0 \end{bmatrix}$ .

Since matrix  $A_i (i = 1, 2, 3)$  satisfies the Hurwitz condition, there must be a positive definite matrix  $P_i (i = 1, 2, 3)$  such that the following equation holds:

$$A_i^T P_i + P_i A_i = -I, (i = 1, 2, 3) \tag{15}$$

where matrix I represents the corresponding identity matrix.

**Hypothesis 1.** *The derivative term  $h_i$  of the extended state in three ESOs with respect to time satisfies  $|h_i| \leq \lambda_i, i = 1, 2, 3$ , where  $\lambda_i$  are unknown positive real numbers representing their boundaries. It is important to note that the three linear extended-state observers have the same structure. It can be inferred from the analysis in [34] and [35] that the observer’s observation error bounds and convergence speeds are related to tunable parameters  $\tau_i (i = 1, 2, 3)$ , and the desired performance can be achieved by adjusting them. We will talk about its stability proof in the next section.*

### 3.4. Design of the DSAADRC

Due to the presence of non-matching disturbances in the system, the backstepping method is used for the design of the controller.

STEP.1: Tracking errors  $e_1$  and  $e_2$  are defined as follows:

$$\begin{cases} e_1 = x_1 - x_d \\ e_2 = \dot{e}_1 + k_1 e_1 = x_2 - x_{2eq} \\ x_{2eq} = -k_1 e_1 + \dot{x}_d \end{cases} \tag{16}$$

That is, when  $e_2$  tends to 0,  $e_1$  must tend to 0. Therefore, the control quantity is designed so that  $e_2$  tends to 0.

STEP.2: The derivative of  $e_2$  with respect to time  $t$  is as follows:

$$\begin{aligned} \dot{e}_2 &= \dot{x}_2 - \dot{x}_{2eq} \\ &= \frac{A}{M} x_3 - \theta_1 x_2 - F(t) - \dot{x}_{2eq} \end{aligned} \tag{17}$$

Design the virtual control signal  $\alpha_3$  for  $x_3$  and define the error  $e_3$  as follows:

$$\begin{cases} e_3 = x_3 - \alpha_3 \\ \alpha_3 = (\alpha_{3a} + \alpha_{3s}) \frac{M}{A} \\ \alpha_{3a} = \hat{\theta}_1 x_2 + \hat{F}(t) + \dot{x}_{2eq} \\ \alpha_{3s} = -k_2 e_2 \end{cases} \tag{18}$$

where  $k_2$  is the adjustable control parameter, and  $\alpha_{3a}$  and  $\alpha_{3s}$  represent the model compensation term and the robust term, respectively. By substituting Equation (18) into Equation (17), the dynamics of  $e_2$  are as follows:

$$\dot{e}_2 = \frac{A}{M} e_3 + \tilde{\theta}_1 x_2 + \tilde{F}(t) - k_2 e_2 \tag{19}$$

STEP.3: Similar to step.2, the design goal is to make  $e_3$  converge to 0. The derivative of  $e_3$  with respect to time  $t$  is as follows:

$$\dot{e}_3 = \dot{x}_3 - \dot{\alpha}_3 = \frac{\beta_e}{V_0} (D_p x_4 - A x_2) - \theta_2 x_3 - Q(t) - \dot{\alpha}_3 \tag{20}$$

$\dot{\alpha}_3$  in Equation (20) includes two parts,  $\dot{\alpha}_{3c}$  and  $\dot{\alpha}_{3u}$ , which represent the calculable and non-calculable parts, respectively, and can be written as follows:

$$\begin{cases} \dot{\alpha}_{3c} = \frac{\partial \alpha_3}{\partial x_2} \left( \frac{A}{M} x_3 - \hat{\theta}_1 x_2 - \hat{F}(t) \right) + \frac{\partial \alpha_3}{\partial \hat{\theta}} \dot{\hat{\theta}} + \frac{\partial \alpha_3}{\partial x_1} x_2 + \frac{\partial \alpha_3}{\partial t} + \frac{\partial \alpha_3}{\partial \hat{F}(t)} \dot{\hat{F}}(t) \\ \dot{\alpha}_{3u} = \frac{\partial \alpha_3}{\partial x_2} (\tilde{\theta}_1 x_2 + \tilde{F}(t)) \end{cases} \quad (21)$$

Design the virtual control signal  $\alpha_4$  for  $x_4$  and define the error  $e_4 = x_4 - \alpha_4$ . The virtual control signal  $\alpha_4$  can be designed as follows:

$$\begin{cases} \alpha_4 = \frac{\alpha_{4a} + \alpha_{4s}}{D_p} \\ \alpha_{4a} = A x_2 + \frac{V_0}{\beta_e} (\dot{\alpha}_{3c} + \hat{\theta}_2 x_3 + \hat{Q}(t)) \\ \alpha_{4s} = -\frac{V_0}{\beta_e} k_3 e_3 \end{cases} \quad (22)$$

The dynamic equation of  $e_3$  can be obtained by combining Equations (20)–(22) as follows:

$$\dot{e}_3 = \frac{\beta_e D_p}{V_0} e_4 + \tilde{\theta}_2 x_3 + \tilde{Q}(t) - \dot{\alpha}_{3u} - k_3 e_3 \quad (23)$$

STEP.4: Similar to the previous step, the derivative of  $e_4$  with respect to time  $t$  is the following:

$$\dot{e}_4 = \dot{x}_4 - \dot{\alpha}_4 = \frac{1}{J_a} \left( k_t \frac{U - k_e x_4}{R} - D_p x_3 \right) - \theta_3 x_4 - T(t) - \dot{\alpha}_4 \quad (24)$$

From Equation (22),  $\alpha_4$  is a function of time  $t$ , the system state vector  $X$ , and the unknown parameter vector  $\theta$ . The “differential explosion” problem can be avoided by adopting a dynamic surface approach to obtain  $\dot{\alpha}_4$ .

Replace  $\alpha_4$  in Equation (22) with  $\bar{x}_4$  and redefine  $\alpha_4$  as the output of  $\bar{x}_4$  through one low-pass filter  $(\rho s + 1)^{-1}$ . Additionally, the conditions listed below are satisfied:

$$\begin{cases} \rho \dot{\alpha}_4 + \alpha_4 = \bar{x}_4 \\ \alpha_4(0) = \bar{x}_4(0) \end{cases} \quad (25)$$

From Equation (25) the following can be further derived:

$$\dot{\alpha}_4 = \frac{\bar{x}_4 - \alpha_4}{\rho} \quad (26)$$

At this point, it is possible to design the control input  $U$  as follows:

$$\begin{cases} U = (U_a + U_s) \frac{R}{k_t} \\ U_a = D_p x_3 + J_a (\hat{\theta}_3 x_4 + \hat{T}(t) + \dot{\alpha}_4) + k_e x_4 \frac{k_t}{R} \\ U_s = -J_a k_4 e_4 \end{cases} \quad (27)$$

Combining Equations (24) and (27), the dynamic equation for  $e_4$  can be rewritten as follows:

$$\dot{e}_4 = \tilde{\theta}_3 x_4 + \tilde{T}(t) - k_4 e_4 \quad (28)$$

The filtering error  $e_5$  can be defined as  $e_5 = \alpha_4 - \bar{x}_4$ . Then, the dynamic equation of  $e_5$  is as follows:

$$\dot{e}_5 = \dot{\alpha}_4 - \dot{\bar{x}}_4 = \frac{\bar{x}_4 - \alpha_4}{\rho} - \dot{\bar{x}}_4 = -\frac{e_5}{\rho} - \dot{\bar{x}}_4 \quad (29)$$

It is noteworthy that according to the definition of the filtering error  $e_5$  and error  $e_4$ , the following can be derived:

$$e_4 = x_4 - (\bar{x}_4 + e_5) \quad (30)$$

Therefore, by combining Equations (20) and (30), the dynamics of  $e_3$  can be rederived as follows:

$$\dot{e}_3 = \frac{\beta_e D_p}{V_0}(e_4 + e_5) + \tilde{\theta}_2 x_3 + \tilde{Q}(t) - \dot{\alpha}_{3u} - k_3 e_3 \tag{31}$$

**Remark 1.** In this study, in order to facilitate the design of control laws, the influence of filtering error on control accuracy in the dynamic surface control method is ignored. But, in fact, such simplified processing will reduce control accuracy to a certain extent. In order to compensate for the loss of control accuracy, a compensation mechanism for filtering errors can be designed [36], that is,  $\zeta$  is introduced and designed as follows:

$$\dot{\zeta} = -L\zeta - 2e_5^2 \text{sgn}(\zeta) + e_5, \zeta(0) = 0 \tag{32}$$

where  $L$  is a positive tunable parameter.

### 3.5. Stability Analysis

The Lyapunov function  $V_a$  is designed as follows:

$$V_a = \sum_{i=1}^5 \frac{1}{2} e_i^2 + \sum_{i=1}^3 \frac{1}{2} \eta_i^T P_i \eta_i + \frac{1}{2} \tilde{\theta}^T \Gamma^{-1} \tilde{\theta} \tag{33}$$

Combining Equations (14), (16), (18), (19), (29) and (31), the derivatives of  $V_a$  with respect to time  $t$  can be obtained as follows:

$$\begin{aligned} \dot{V}_a &= \left( \sum_{i=1}^5 \frac{1}{2} \dot{e}_i^2 + \sum_{i=1}^3 \frac{1}{2} \dot{\eta}_i^T P_i \eta_i + \frac{1}{2} \dot{\tilde{\theta}}^T \Gamma^{-1} \tilde{\theta} \right)' \\ &= e_1(e_2 - k_1 e_1) + e_2 \left( \frac{A}{M} e_3 + \tilde{\theta}_1 x_2 + \tilde{F}(t) - k_2 e_2 \right) + e_3 \left[ \frac{\beta_e D_p}{V_0} (e_4 + e_5) + \tilde{\theta}_2 x_3 + \tilde{Q}(t) - \dot{\alpha}_{3u} - k_3 e_3 \right] \\ &+ e_4 (\tilde{\theta}_3 x_4 + \tilde{T}(t) - k_4 e_4) + e_5 \left( -\frac{e_5}{\rho} - \dot{\tilde{x}}_4 \right) - \frac{1}{2} \tau_1 \|\eta_1\|^2 - \eta_1^T P_1 B_1 \frac{\tilde{\theta}_1 x_2}{\tau_1} - \frac{1}{2} \tau_2 \|\eta_2\|^2 - \eta_2^T P_2 C_1 \tilde{\theta}_2 x_3 \\ &- \frac{1}{2} \tau_3 \|\eta_3\|^2 - \eta_3^T P_3 D_1 \tilde{\theta}_3 x_4 + \tilde{\theta}^T \Gamma^{-1} \dot{\tilde{\theta}} - \eta_1^T P_1 B_2 \frac{h_1(t)}{\tau_1^2} - \eta_2^T P_2 C_2 \frac{h_2(t)}{\tau_2} - \eta_3^T P_3 D_2 \frac{h_3(t)}{\tau_3} \end{aligned} \tag{34}$$

Suppose there exists an upper bound  $M_2$  for  $\dot{\tilde{x}}_4$ , i.e.,  $|\dot{\tilde{x}}_4| < M_2$ .

The adaptive law  $\dot{\tilde{\theta}}$  can be designed as follows:

$$\begin{cases} \dot{\tilde{\theta}} = \varphi_1 x_2 + \varphi_2 x_3 + \varphi_3 x_4 \\ \varphi_1 = [-e_2 + \frac{\eta_1^T P_1 B_1}{\tau_1} + \frac{\partial \alpha_3}{\partial x_2} e_3 - \frac{\hat{\theta}_1}{\delta_1}, 0, 0]^T \\ \varphi_2 = [0, -e_3 + \eta_2^T P_2 C_1 - \frac{\hat{\theta}_2}{\delta_2}, 0]^T \\ \varphi_3 = [0, 0, -e_4 + \eta_3^T P_3 D_1 - \frac{\hat{\theta}_3}{\delta_3}]^T \end{cases} \tag{35}$$

where  $\delta_i > 0$  ( $i = 1, 2, 3$ ) is the gain parameter. Substituting Equation (35) into Equation (34), based on Young's inequality [37], the following can be inferred:

$$\begin{aligned} \dot{V}_a &\leq -k_1 e_1^2 - k_2 e_2^2 - k_3 e_3^2 - k_4 e_4^2 - \left( \frac{1}{\rho} - \frac{M_2^2}{2\mu} \right) e_5^2 \\ &+ |e_1| |e_2| + \frac{A}{M} |e_2| |e_3| + \frac{\beta_e D_p}{V_0} (|e_3| |e_4| + |e_3| |e_5|) \\ &+ \tau_1^2 |e_2| |\eta_{13}| + \tau_2 |e_3| |\eta_{22}| + \tau_3 |e_4| |\eta_{32}| + \tau_1^2 \left| \frac{\partial \alpha_3}{\partial x_2} \right| |e_3| |\eta_{13}| \\ &- \frac{1}{2} (\tau_1 - 1) \|\eta_1\|^2 - \frac{1}{2} (\tau_2 - 1) \|\eta_2\|^2 - \frac{1}{2} (\tau_3 - 1) \|\eta_3\|^2 \\ &+ \left( \|P_1 B_2\| \frac{|h_1(t)|_{\max}}{\tau_1^2} \right)^2 + \left( \|P_2 C_2\| \frac{|h_2(t)|_{\max}}{\tau_2} \right)^2 \\ &+ \left( \|P_3 D_2\| \frac{|h_3(t)|_{\max}}{\tau_3} \right)^2 + \frac{\mu}{2} + \frac{\hat{\theta}_1^2}{\delta_1} + \frac{\hat{\theta}_2^2}{\delta_2} + \frac{\hat{\theta}_3^2}{\delta_3} + \tilde{\theta}_1^2 + \tilde{\theta}_2^2 + \tilde{\theta}_3^2 \end{aligned} \tag{36}$$

where the parameter  $\mu > 0$ . Equation (36) can be further simplified as follows:

$$\begin{aligned} \dot{V}_a &\leq -Z^T \Lambda Z + \varepsilon \\ &\leq -\lambda_{\min}(\Lambda)(\|e^T\|^2 + \sum_{i=1}^3 \|\eta_i^T\|^2 + \|\tilde{\theta}^T\|^2) + \varepsilon \\ &\leq -\lambda_{\min}(\Lambda)(\sum_{i=1}^5 e_i^2 + \sum_{i=1}^3 \frac{1}{\lambda_{\max}(P_i)} \eta_i^T P_i \eta_i + \frac{1}{\lambda_{\max}(\Gamma^{-1})} \tilde{\theta}^T \Gamma^{-1} \tilde{\theta}) + \varepsilon \\ &\leq -\lambda_a V_a + \varepsilon \end{aligned} \tag{37}$$

The results that can be obtained after resolving this inequality are as follows:

$$V_a(t) \leq V_a(0) \exp(-\lambda_a t) + \frac{\varepsilon}{\lambda_a} [1 - \exp(-\lambda_a t)] \tag{38}$$

According to Equation (38), the closed-loop system's parameters are all bounded by the control law in Equation (27), and the gain parameter can change this constraint.

In Equation (37),  $Z^T = [e^T, \eta_1^T, \eta_2^T, \eta_3^T, \tilde{\theta}^T]$ , there are as follows:

$$\varepsilon = (\|P_1 B_2\| \frac{|h_1(t)|_{\max}}{\tau_1^2})^2 + (\|P_2 C_2\| \frac{|h_2(t)|_{\max}}{\tau_2})^2 + (\|P_3 D_2\| \frac{|h_3(t)|_{\max}}{\tau_3})^2 + \frac{\mu}{2} + \frac{\hat{\theta}_1^2}{\delta_1} + \frac{\hat{\theta}_2^2}{\delta_2} + \frac{\hat{\theta}_3^2}{\delta_3}, \quad \Lambda = \begin{bmatrix} \Lambda_1 & \Lambda_{12} & \Lambda_{13} & \Lambda_{14} & 0 \\ \Lambda_{12}^T & \Lambda_3 & 0 & 0 & 0 \\ \Lambda_{13}^T & 0 & \Lambda_4 & 0 & 0 \\ \Lambda_{14}^T & 0 & 0 & \Lambda_5 & 0 \\ 0 & 0 & 0 & 0 & \Lambda_2 \end{bmatrix},$$

$$\Lambda_1 = \begin{bmatrix} k_1 & -\frac{1}{2} & 0 & 0 & 0 \\ -\frac{1}{2} & k_2 & -\frac{A}{2M} & 0 & 0 \\ 0 & -\frac{A}{2M} & k_3 & -\frac{D_p \beta_e}{2V_0} & -\frac{D_p \beta_e}{2V_0} \\ 0 & 0 & -\frac{D_p \beta_e}{2V_0} & k_4 & 0 \\ 0 & 0 & -\frac{D_p \beta_e}{2V_0} & 0 & \frac{1}{\rho} - \frac{M_2^2}{2\mu} \end{bmatrix}, \quad \Lambda_2 = \frac{1}{2} \begin{bmatrix} 1 & 0 & 0 \\ 0 & 1 & 0 \\ 0 & 0 & 1 \end{bmatrix},$$

$$\Lambda_3 = \frac{1}{2} \begin{bmatrix} \tau_1 - 1 & 0 & 0 \\ 0 & \tau_1 - 1 & 0 \\ 0 & 0 & \tau_1 - 1 \end{bmatrix}, \quad \Lambda_4 = \frac{1}{2} \begin{bmatrix} \tau_2 - 1 & 0 \\ 0 & \tau_2 - 1 \end{bmatrix}, \quad \Lambda_5 = \frac{1}{2} \begin{bmatrix} \tau_3 - 1 & 0 \\ 0 & \tau_3 - 1 \end{bmatrix},$$

$$\Lambda_{12} = \frac{-\tau_1^2}{2} \begin{bmatrix} 0 & 0 & 0 \\ 0 & 0 & 1 \\ 0 & 0 & \left| \frac{\partial \alpha_3}{\partial x_2} \right| \\ 0 & 0 & 0 \\ 0 & 0 & 0 \end{bmatrix}, \quad \Lambda_{13} = \frac{-\tau_2}{2} \begin{bmatrix} 0 & 0 \\ 0 & 1 \\ 0 & 0 \\ 0 & 0 \\ 0 & 0 \end{bmatrix}, \quad \Lambda_{14} = \frac{-\tau_3}{2} \begin{bmatrix} 0 & 0 \\ 0 & 1 \\ 0 & 0 \\ 0 & 0 \\ 0 & 0 \end{bmatrix},$$

$$\lambda_a = 2\lambda_{\min}(\Lambda) \min\left\{1, \frac{1}{\lambda_{\max}(P_1)}, \frac{1}{\lambda_{\max}(P_2)}, \frac{1}{\lambda_{\max}(P_3)}, \frac{1}{\lambda_{\max}(\Gamma^{-1})}\right\},$$

where  $\lambda_{\min}(\bullet)$  and  $\lambda_{\max}(\bullet)$  represent the minimum and maximum eigenvalues of  $\bullet$ , respectively.

### 4. Simulation Analysis

Three sets of simulation experiments are created for comparative analysis in order to confirm the efficacy and superiority of the above-designed control strategy. The desired input  $x_d$  is given as  $x_d = 0.04 \sin(\pi t)[1 - \exp(-t^3)]$ . The four controllers are as follows:

- (1) The DSAADRC controller is proposed in this paper. In this set of simulations, the controller parameters used are the following: gain matrix  $\Gamma = \text{diag}\{5000, 6.2 \times 10^{-11}, 3.5 \times 10^{-4}\}$ ; ESO gain  $\tau_i = (200, 500, 1000)$ , ( $i = 1, 2, 3$ ); gain parameter  $\delta_i = 1000$ , ( $i = 1, 2, 3$ ); feedback gain  $k_i = (100, 50, 155, 227)$ , and ( $i = 1, 2, 3, 4$ ); filter parameter  $\rho = 0.01$ . The upper and lower limits of the parameters are set to  $\theta_{\max} = [40, 150, 20]$  and  $\theta_{\min} = [0, 0, 0]$ . Since the parameters' actual values are unknown, it might be helpful to set the initial estimates of the parameters to  $\hat{\theta} = [0, 0, 0]$ .
- (2) The Backstepping Robust Controller (RC), which has the same feedback gain as DSAADRC. Compared to DSAADRC, it also has the same model compensation term, but without the parameter adaptive function and ESO.
- (3) Adaptive Robust Controller (ARC). Although this controller gives the RC an adaptive function, it lacks the ESO's external disturbance compensation effect. Its adaptive parameter gain and feedback gain are the same as those of DSAADRC.

Table 1 lists the primary variables used for the EHA position servo simulation.

**Table 1.** Simulative parameters of the EHA.

Parameters	Values
Piston effective area $A$ (m <sup>2</sup> )	$1.134 \times 10^{-3}$
Effective stroke $L_e$ (m)	0.1
Leakage coefficient $L_c$ (m <sup>3</sup> /(s/Pa))	$2.5 \times 10^{-11}$
Elastic modulus of oil $\beta_e$ (N/m <sup>2</sup> )	$6.86 \times 10^8$
Total cylinder volume $V_0$ (m <sup>3</sup> )	$4 \times 10^{-4}$
Viscous friction coefficient of the cylinder $B_c$ (N/(m/s))	1000
Mass of cylinder and load $M$ (kg)	243
Pump Displacement $D_p$ (m <sup>3</sup> /rad)	$3.98 \times 10^{-7}$
Viscous friction coefficient of the motor $B_m$ (N·m/(rad/s))	$6 \times 10^{-4}$
Phase resistance $R$ ( $\Omega$ )	0.2
Phase Inductance $L$ (mH)	1.33
Inertia of the spindle $J_a$ (kg·m <sup>2</sup> )	$4 \times 10^{-4}$
Torque coefficient $K_t$ (N·m/A)	0.351
Factor of back EMF $K_e$ (V/(rad/s))	0.234
Elastic load factor $K_s$ (N/m)	0
Bus voltage $U$ (VDC)	270

Figure 2 displays the simulation outcomes for the position tracking error for the three control methods. The estimation results of ESO and the adaptive convergence results of unknown parameters in DSAADRC are also shown in Figures 3 and 4, respectively. It should be noted that after several iterations of parameter tuning, the obtained simulation results can be seen in Figure 2. The first error waveform is the same for both RC and ARC, and the tracking error for ARC gradually decreases to less than 0.2 mm from the second waveform, reflecting the influence of adaptive law. It can be seen from a comparison of DSAADRC and ARC that ESO has a positive impact on estimating the uncertainty perturbation in the system, which is also evident from Figure 3. Additionally, the accumulation of feedforward compensation has improved the ability of DSAADRC to suppress outside disturbances.

To further verify the effectiveness of the proposed DSAADRC method, a perturbation is injected to the control signal at 10 s with a disturbance value of  $u_d = 10 + 100x_d$ . Its tracking error and ESO for perturbation estimation simulation results are displayed in Figures 5 and 6, respectively. When the system input signal is perturbed, as shown in Figures 2 and 5, the position tracking error curves of RC and ARC are significantly shifted, with the maximum tracking error increasing from 0.4 mm and 0.2 mm to approximately 2 mm, while the tracking error of the proposed DSAADRC method stays within 0.2 mm. This disturbance acts on the control input signal, which is equivalent to artificially adding a perturbation to the fourth channel of Equation (6), i.e., assigning a value to  $T(t)$ . Combining this with Figure 6, it is also evident that at the 10th s, the ESO of both  $Q(t)$  and  $F(t)$  do not exhibit discernible significant fluctuations, while the observations of  $T(t)$  are able to track

their actual changes. This demonstrates that the DSAADRC method is able to estimate and account for the disturbances in the system inputs with ESO, significantly enhancing the system's robustness.

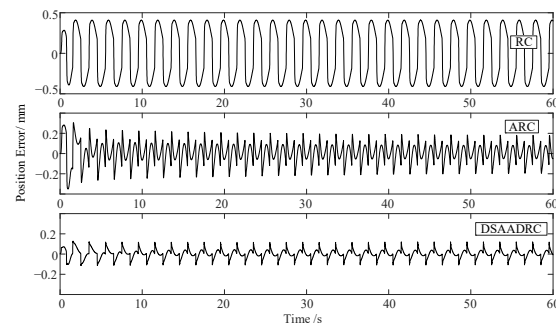


**Figure 2.** Tracking error of the sinusoidal signal in RC, ARC, and DSAADRC.

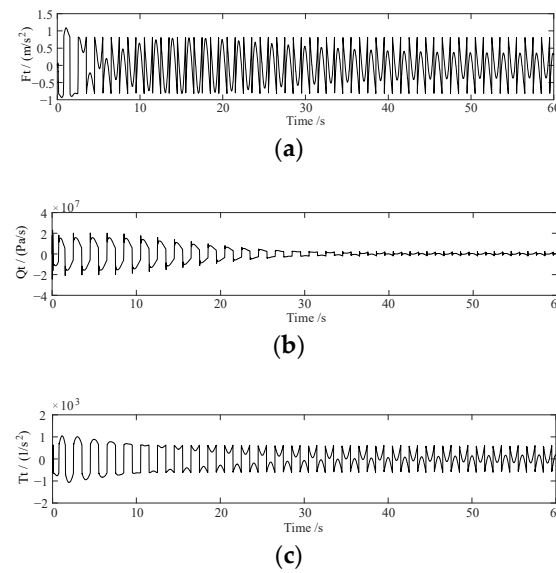


**Figure 3.** Estimated results of ESO. (a) Estimate of  $F_t$ ; (b) Estimate of  $Q_t$ ; (c) Estimate of  $T_t$ .

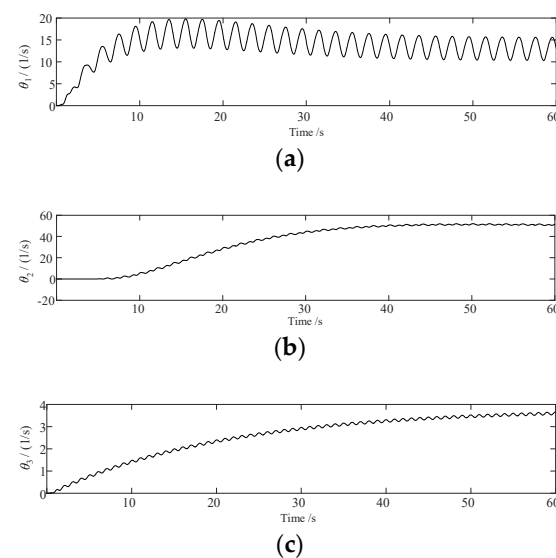


**Figure 4.** Adaptive results for unknown parameters. (a) Estimate of  $\theta_1$ ; (b) Estimate of  $\theta_2$ ; (c) Estimate of  $\theta_3$ .

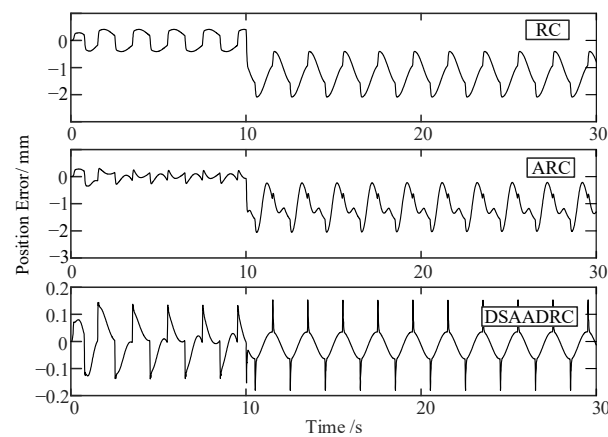


**Figure 5.** Tracking error of the sinusoidal signal under disturbance in RC, ARC, and DSAADRC.

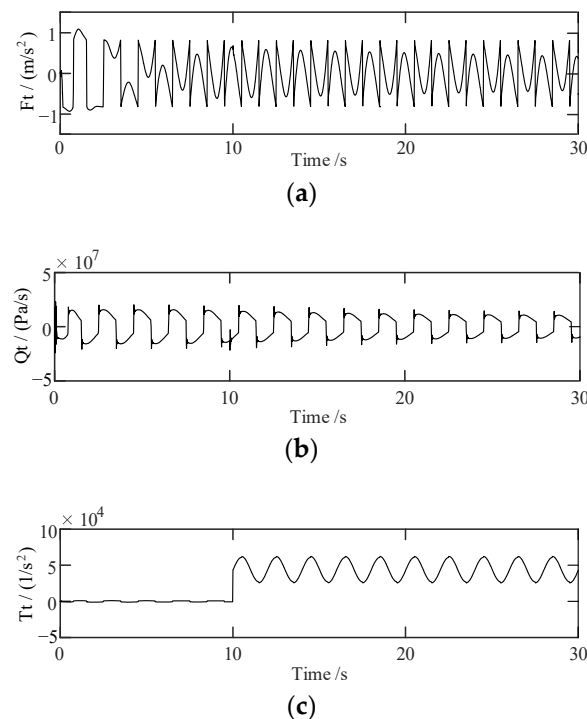


**Figure 6.** Estimated results of ESO under disturbance. (a) Estimate of  $F_t$ ; (b) Estimate of  $Q_t$ ; (c) Estimate of  $T_t$ .

## 5. Experimental Verification

### 5.1. Test Bench

An EHA prototype and test platform, as shown in Figure 7, were established in order to validate the suggested control method. A position sensing element is used to detect actuator displacement, while the sensor signals are fed to the controller through an SG37-2-09.52 encoder. In addition, two pressure sensors are employed to monitor the pressure in the two chambers of the piston cylinder. The regulating valves are performed for mode switching in operation. Table 2 displays the EHA prototype's specifications.

Figure 7 displays the main components of the experimental platform. The control commands, with a sampling rate of 200 Hz, were originally executed on a host computer as reference inputs, which are compliant with the computational simulation. The power electronics are set up for signal exchange and processing. Control commands are delivered from the host computer to the power electronics and then to the EHA as inputs. Specifically, the motor driving signals and valve signals together constitute the inputs to the EHA system. The former is generated by integrating control commands and system feedback

signals, while the latter changes the mode of operation. The feedback signals from the EHA system, containing the motor current and displacement of the actuator, are fed back to the host computer via the power electronics. The feedback data used in this experiment are derived from a second-order Butterworth filter with a cutoff frequency of 40 Hz, which is five times the referenced bandwidth of the EHA [8].

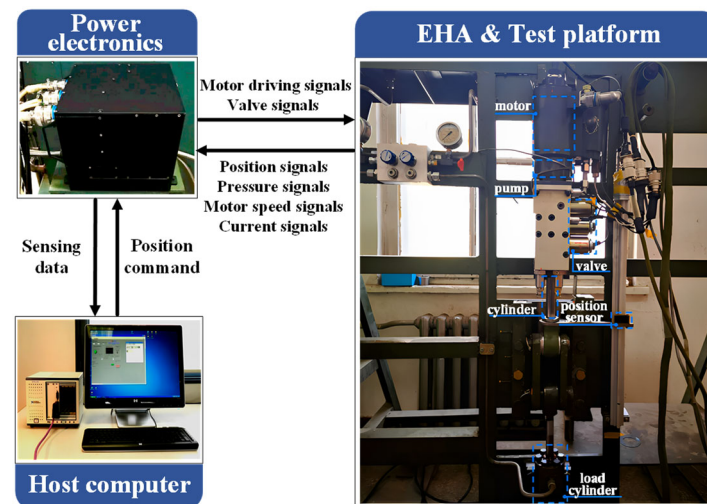


Figure 7. EHA experimental platform.

Table 2. Parameters of the EHA prototype.

Parameters	Values
Rated pressure (MPa)	11
Rated speed (mm/s)	300
Rated load (kN)	12
Effective stroke (mm)	110
Rated voltage (VDC)	270
Bandwidth (Hz)	5

## 5.2. Results

The EHA studied is used for aileron actuation in medium-sized civil airliners. As an actuator of the primary flight control rudder surface, it is mainly used to continuously adjust the output displacement according to the instructions of the flight control computer during the take-off and landing of the passenger aircraft and then adjust the deflection angle of the rudder surface. Take the Airbus A320, a typical medium-sized civilian airliner as an example. Its aileron actuator has a stroke of 44 mm and a bandwidth of about 1 Hz, but it should be noted that the indicators here correspond to the worst-case scenario. In reality, under normal circumstances, actuation functions operate well below these extreme values. During the course of a typical mission, only  $-80$  to  $20\%$  of the available force and  $\pm 15\%$  of the available speed are used [38]. Therefore, the desired input signal here is given as  $x_d = 0.01\sin(\pi t)$ , which is a sinusoidal signal with an amplitude of 10 mm and a frequency of 0.5 Hz. The EHA position tracking errors under various methods are shown in Figure 8 as a result of the position servo control experiments that were conducted on the EHA control methods of RC, ARC, and DSAADRC, respectively.

As seen in Figure 8, when the results of RC and ARC are compared, it is discovered that both controllers have a tracking error of approximately 1.7 mm at the starting stage; however, the tracking error of ARC tends to converge over time as a result of the adaptive estimation of parameters. The parameters of the adaptive gain matrix are correlated with the convergence rate at 35 s, and the tracking error converges to 1.5 mm. This indicates that the designed adaptive law can modify the unknown parameters of the system online, which is advantageous to enhance the tracking performance. While the RC lacks the ability

to learn and correct unknown parameters online. As a result, for a constant external load, the position tracking errors of the RC controller at 0 s and 35 s are essentially unchanged.

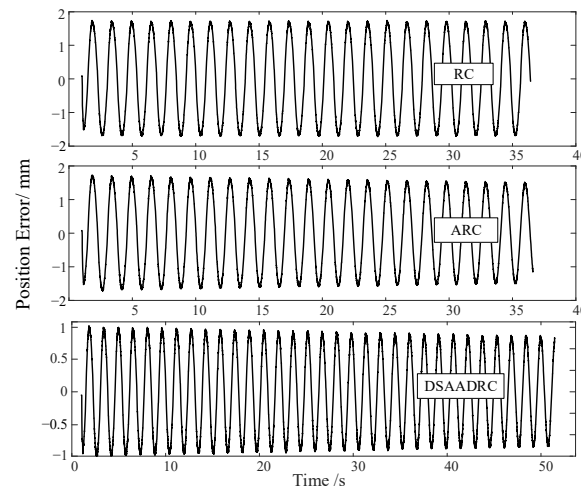


**Figure 8.** Tracking error of the sinusoidal signal in RC, ARC, and DSAADRC (Experimental results).

Further, comparing the experimental results of DSAADRC and ARC controllers, it is found that the tracking errors of both converge gradually with time, while the tracking error of the former at the starting moment is 1 mm, which is much smaller than that of the latter at 1.7 mm. This suggests that the estimation and advance compensation effect of the ESO on the external load results in a much lighter task for the robust term, increasing the system’s tracking accuracy.

In order to further quantitatively evaluate the performance of the three controllers, the tracking errors of the last two cycles in the experimental results were quantitatively analyzed using the following four performance indicators, which were defined as follows:

- (1) Maximum absolute error (MAE)

$$E_m = \max_{i=1, \dots, N} \{|e(i)|\} \tag{39}$$

where  $N$  is the number of signal points. MAE reflects the magnitude of the absolute value of the following error.

- (2) Average absolute error (AAE)

$$u_e = \frac{1}{N} \sum_{i=1}^N |e(i)| \tag{40}$$

- (3) Standard deviation of error (SDE)

$$S_e = \sqrt{\frac{1}{N} \sum_{i=1}^N [ |e(i)| - u_e ]^2} \tag{41}$$

SDE reflects the convergence speed of the controller, i.e., the smaller the value, the faster the convergence.

- (4) Average time-weighted absolute error (ATAE) [39,40]

$$\mu_e = \frac{1}{N} \sum_{i=1}^N (i|e(i)|) \tag{42}$$

ATAE focuses more on the error size after the system enters a steady state.

The above four performance indices are used to fairly compare the tracking performance of different controllers. It should be noted that the smaller the value of the four indices, the better the tracking performance. Table 3 displays the comparison results, which clearly demonstrate that the DSAADRC method outperforms the other two controllers in each of the four evaluation indices.

**Table 3.** Tracking performance indices of three controllers.

	$E_m$ (mm)	$S_e$ (mm)	$u_e$ (mm)	$\mu_e$ (mm)
RC	1.73	0.0438	0.0552	917.78
ARC	1.54	0.038	0.0476	816.28
DSAADRC	0.84	0.0316	0.0406	436.72

The estimation results of ESO in the DSAADRC are shown in Figure 9. By analyzing the estimation results of the three observers, it can be concluded that the largest influence on the EHA displacement is  $F_t$ , which also confirms the role of the observer's estimation in improving the system's accuracy.

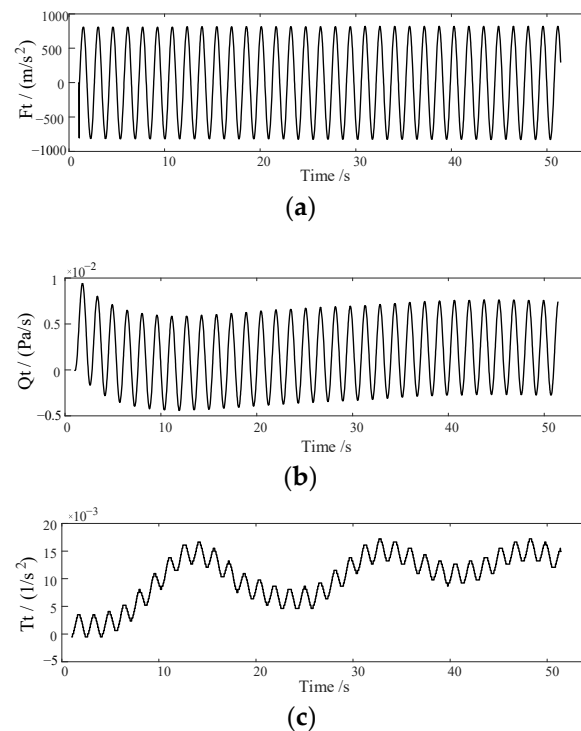


**Figure 9.** Estimated results of ESO (experimental results). (a) Estimate of  $F_t$ ; (b) Estimate of  $Q_t$ ; (c) Estimate of  $T_t$ .

The outcomes of parameter adaptation in DSAADRC are depicted in Figure 10, and it is clear that  $\theta_2$  has converged to almost a fixed value,  $\theta_3$  exhibits a trend of convergence, whereas  $\theta_1$  is still in the process of convergence, which explains why the tracking error of DSAADRC in Figure 8 is still in the convergence state.

It is true that the speed of parameter convergence can be improved by increasing the parameters of the adaptive matrix, but since there is also an estimate of  $\theta$  in ESO, excessive adaptive gain will negatively impact the observational results of ESO, which will affect the systematic error and thus affect the process of parameter adaptation. In practical experiments, the estimation of unknown parameters by the adaptive law and the observation of perturbations by the ESO are mutually coupled processes that necessitate numerous parameter adjustments and iterations in order to ensure accurate ESO estimation and convergence of adaptive parameters while taking into account the system's good

tracking performance. This outcome is still adequate to demonstrate the superiority and potential of the DSAADRC, though.

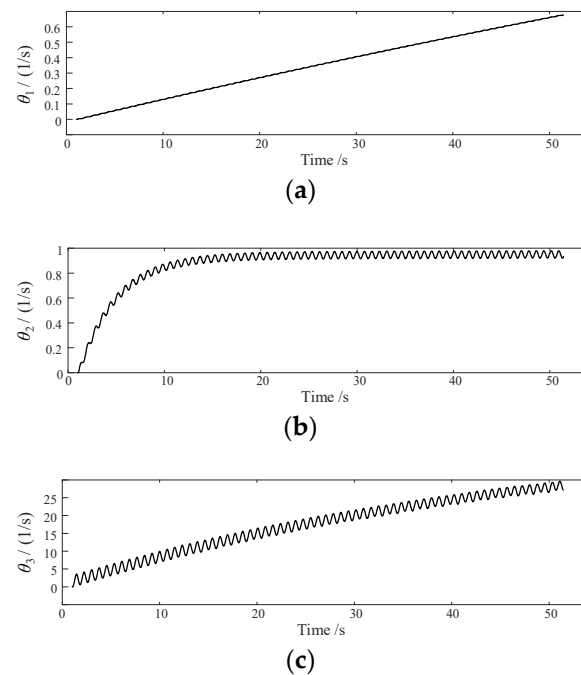


**Figure 10.** Adaptive results for unknown parameters (experimental results). (a) Estimate of  $\theta_1$ ; (b) Estimate of  $\theta_2$ ; (c) Estimate of  $\theta_3$ .

## 6. Conclusions

This study develops an EHA dynamics model with uncertain parameters and disturbance terms. An adaptive active anti-disturbance control method based on dynamic surfaces is designed using the framework of the backstepping method to address the issue that non-matching disturbance, parameter uncertainty, and disturbance uncertainty in the system cause the EHA control accuracy and stability to degrade. It is shown that all parameters of the closed-loop system are bounded based on Lyapunov stability theory, which is verified by simulation and experiment. The conclusions that follow are attained.

- (1) The benefits of the proposed dynamic surface-based adaptive active disturbance rejection control method include estimating external disturbances, overcoming parameter uncertainties, and preventing “differential explosion”. This method combines dynamic surfaces, adaptive robust control, and ESO. Even in the presence of time-varying external disturbances, it can guarantee the position tracking accuracy of EHA.
- (2) Two techniques, namely robust control and adaptive robust control, were compared and used to verify DSAADRC. The simulation and experiment results demonstrate that DSAADRC was superior in three evaluation indices, including maximum absolute error  $E_m$ , average standard deviation  $S_e$ , and average error  $u_e$ , which indicate the effectiveness of the method in suppressing disturbances and the superiority in improving the accuracy of EHA position tracking.

Despite the above advantages, the designed DSAADRC method still has shortcomings, particularly in terms of the number of parameters to be tuned and the absence of clear guidelines and methods. Because of its quick and efficient parameter tuning method, it is still valuable to study in depth.

**Author Contributions:** Conceptualization, Y.W. and X.H.; Methodology, X.H. and M.W.; Resources, D.Z.; Validation, M.W. and X.H.; Data curation, M.W.; Writing—original draft preparation, X.H.; Writing—review and editing, Y.F. and Y.W.; project administration, Y.F. All authors have read and agreed to the published version of the manuscript.

**Funding:** This research received no external funding.

**Data Availability Statement:** The data presented in this study are available on request from the corresponding author.

**Conflicts of Interest:** The authors declare no conflict of interest.

## References

1. Ercan, H.; Akin, M. Performance analysis of electrical flight control actuation system in a commercial transport aircraft. *Aircr. Eng. Aerosp. Technol.* **2022**, *94*, 1671–1683. [[CrossRef](#)]
2. Bae, J. A Review of Electric Actuation and Flight Control System for More/All Electric Aircraft. In Proceedings of the 2021 24th International Conference on Electrical Machines and Systems, Gyeongju, Republic of Korea, 31 October–3 November 2021.
3. Chao, Q.; Zhang, J.; Xu, B. A Review of High-Speed Electro-Hydrostatic Actuator Pumps in Aerospace Applications: Challenges and Solutions. *J. Mech. Des.* **2019**, *141*, 050801. [[CrossRef](#)]
4. Habibi, S.; Goldenberg, A. Design of a new high-performance electrohydraulic actuator. *IEEE/ASME Trans. Mechatron.* **2000**, *5*, 158–164. [[CrossRef](#)]
5. Gao, B.; Fu, Y.; Pei, Z. Research on dual-variable integrated electro-hydrostatic actuator. *China J. Aeronaut.* **2006**, *19*, 77–82. [[CrossRef](#)]
6. Zhang, Y.; Fu, Y.; Zhou, W. Optimal control for EHA-VPVM system based on feedback linearization theory. In Proceedings of the 11th International Conference on Control, Automation, Robotics and Vision, Singapore, 7–10 December 2010.
7. Kumar, M. A survey on electro hydrostatic actuator: Architecture and way ahead. *Mater. Today-Proc.* **2021**, *45*, 6057–6063. [[CrossRef](#)]
8. Wang, M.; Wang, Y.; Yang, R. A Sliding Mode Control Strategy for an ElectroHydrostatic Actuator with Damping Variable Sliding Surface. *Actuators* **2021**, *10*, 3. [[CrossRef](#)]
9. Wang, Y.; Wang, M.; Fu, J. Adaptive Control of an Aerospace Electrohydrostatic Actuator with a Constant-Torque Variable-Displacement Pump. *J. Aerosp. Eng.* **2022**, *35*, 04022028. [[CrossRef](#)]
10. Wang, S.; Burton, R.; Habibi, S. Sliding Mode Controller and Filter Applied to an Electrohydraulic Actuator System. *J. Dyn. Syst. Trans. ASME* **2011**, *133*, 024504. [[CrossRef](#)]
11. Lee, J.M.; Park, S.H.; Kim, J.S. Design and Experimental Evaluation of a Robust Position Controller for an Electrohydrostatic Actuator Using Adaptive Antiwindup Sliding Mode Scheme. *Sci. World J.* **2013**, *2013*, 590708. [[CrossRef](#)]
12. Ahn, K.K.; Nam, D.N.C.; Jin, M.L. Adaptive Backstepping Control of an Electrohydraulic Actuator. *IEEE/ASME Trans. Mechatron.* **2014**, *19*, 987–995. [[CrossRef](#)]
13. Nie, Y.; Liu, J.; Lao, Z.H. Modeling and Extended State Observer-Based Backstepping Control of Underwater Electro Hydrostatic Actuator with Pressure Compensator and External Load. *Electronics* **2022**, *11*, 1286. [[CrossRef](#)]
14. Li, L.; Wang, M.; Yang, R. Adaptive Damping Variable Sliding Mode Control for an Electrohydrostatic Actuator. *Actuators* **2021**, *10*, 83. [[CrossRef](#)]
15. Yang, R.; Fu, Y.; Zhang, L. A Novel Sliding Mode Control Framework for Electrohydrostatic Position Actuation System. *Math. Probl. Eng.* **2018**, *2018*, 7159891. [[CrossRef](#)]
16. Yao, B.; Tomizukai, M. Adaptive Robust Control of SISO Nonlinear Systems in a Semistrict Feedback Form. *Automatica* **1997**, *33*, 893–903. [[CrossRef](#)]
17. Wang, C.; Quan, L.; Jiao, Z. Nonlinear Adaptive Control of Hydraulic System with Observing and Compensating Mismatching Uncertainties. *IEEE Trans. Control. Syst. Technol.* **2018**, *26*, 927–937. [[CrossRef](#)]
18. Yao, Z.; Yao, J.; Yao, F. Model reference adaptive tracking control for hydraulic servo systems with nonlinear neural-networks. *ISA Trans.* **2020**, *3*, 396–404. [[CrossRef](#)] [[PubMed](#)]
19. Xu, Z.; Qi, G.; Liu, Q. ESO-based adaptive full state constraint control of uncertain systems and its application to hydraulic servo systems. *Mech. Syst. Signal Process.* **2022**, *167*, 108560. [[CrossRef](#)]
20. Choi, H. LMI-Based sliding surface design for integral sliding mode control of mismatched uncertain systems. *IEEE Trans. Autom. Control* **2007**, *52*, 736–742. [[CrossRef](#)]
21. Wen, C.; Cheng, C. Design of sliding surface for mismatched uncertain systems to achieve asymptotical stability. *J. Frankl. Inst. Eng. Appl. Math.* **2008**, *345*, 926–941. [[CrossRef](#)]
22. Yang, J.; Chen, W.; Li, S. Nonlinear disturbance observer-based robust control for systems with mismatched disturbances/uncertainties. *IET Control Theory Appl.* **2011**, *5*, 2053–2062. [[CrossRef](#)]
23. Li, S.; Yang, J.; Chen, W. Generalized extended state observer based control for systems with mismatched uncertainties. *IEEE Trans. Ind. Electron.* **2012**, *59*, 4792–4802. [[CrossRef](#)]
24. Pu, Z.; Yuan, R.; Yi, J. A class of adaptive extended state observers for nonlinear disturbed systems. *IEEE Trans. Ind. Electron.* **2015**, *62*, 5858–5869. [[CrossRef](#)]
25. Yang, X.; Wang, X.; Wang, S. Adaptive Backstepping Control of Uncertain Electro-Hydrostatic Actuator with Unknown Dead-zone Nonlinearity. In Proceedings of the 2021 IEEE 16th Conference on Industrial Electronics and Applications, Chengdu, China, 1–4 August 2021.

26. Swaroop, D.; Hedrick, J.K.; Yip, P.P. Dynamic surface control for a class of nonlinear systems. *IEEE Trans. Autom. Control* **2000**, *45*, 1893–1899. [[CrossRef](#)]
27. Le, D.; Pietrzak, B.W.; Shaver, G.M. Dynamic surface control of a piezoelectric fuel injector during rate shaping. *Control Eng. Pract.* **2014**, *30*, 12–26. [[CrossRef](#)]
28. Farrell, J.A.; Polycarpou, M.; Sharma, M. Command filtered backstepping. *IEEE Trans. Autom. Control* **2009**, *54*, 1391–1395. [[CrossRef](#)]
29. Yu, J.; Shi, P.; Dong, W. Observer and command filter-based adaptive fuzzy output feedback control of uncertain nonlinear systems. *IEEE Trans. Ind. Electron.* **2015**, *62*, 5962–5970. [[CrossRef](#)]
30. Zhang, J.; Wu, J.; Liu, J.; Zhou, Q.; Xia, J.; Sun, W.; He, X. Command-filter-adaptive-based lateral motion control for autonomous vehicle. *Control Eng. Pract.* **2022**, *121*, 105044. [[CrossRef](#)]
31. Butt, W.A.; Yan, L.; Kendrick, A.S. Robust Adaptive Dynamic Surface Control of a Hypersonic Flight Vehicle. In Proceedings of the 49th IEEE Conference on Decision and Control (CDC), Atlanta, GA, USA, 15–17 December 2010; pp. 3632–3637.
32. Butt, W.A.; Yan, L.; Kendrick, A.S. Adaptive dynamic surface control of a hypersonic flight vehicle with improved tracking. *Asian J. Control* **2013**, *15*, 594–605. [[CrossRef](#)]
33. Xu, B.; Huang, X.; Wang, D. Dynamic surface control of constrained hypersonic flight models with parameter estimation and actuator compensation. *Asian J. Control* **2014**, *16*, 162–174. [[CrossRef](#)]
34. Zheng, Q.; Gao, L.; Gao, Z. On stability analysis of active disturbance rejection control for nonlinear time-varying plants with unknown dynamics. In Proceedings of the 46th IEEE Conference on Decision and Control, New Orleans, LA, USA, 12–14 December 2007.
35. Liu, K.; Li, H.; Zhang, Y. Extended state observer based adaptive sliding mode tracking control of wheeled mobile robot with input saturation and uncertainties. *Proc. Inst. Mech. Eng. Part C J. Mech. Eng. Sci.* **2019**, *233*, 5460–5476. [[CrossRef](#)]
36. Liu, K.; Wang, R. Antisaturation Command Filtered Backstepping Control-Based Disturbance Rejection for a Quadrotor UAV. *IEEE Trans. Circuits Syst. II* **2021**, *68*, 3577–3581. [[CrossRef](#)]
37. Sababheh, M.; Choi, D. A complete refinement of Young’s inequality. *J. Math. Anal. Appl.* **2016**, *440*, 379–393. [[CrossRef](#)]
38. Mare, J.C. *Aerospace Actuators 1: Needs, Reliability and Hydraulic Power Solutions*; John Wiley & Sons: Hoboken, NJ, USA, 2016.
39. Liu, K.; Wang, R.; Wang, X. Anti-saturation adaptive finite-time neural network based fault-tolerant tracking control for a quadrotor UAV with external disturbances. *Aerosp. Sci. Technol.* **2021**, *115*, 106790. [[CrossRef](#)]
40. Liu, K.; Wang, R.; Zheng, S. Fixed-time disturbance observer-based robust fault-tolerant tracking control for uncertain quadrotor UAV subject to input delay. *Nonlinear Dynam.* **2022**, *107*, 2363–2390. [[CrossRef](#)]

**Disclaimer/Publisher’s Note:** The statements, opinions and data contained in all publications are solely those of the individual author(s) and contributor(s) and not of MDPI and/or the editor(s). MDPI and/or the editor(s) disclaim responsibility for any injury to people or property resulting from any ideas, methods, instructions or products referred to in the content.